Tutor/s
Dr. Jordi Ignés Mullol
Departament de Ciència de Materials i Química Física

Grau de Química

Treball Final de Grau

Physicochemical processes under microfluidic conditions.
Processos fisicoquímics en condicions microfluídiques.

Júlia Estrades Bestit

June 2024

Universitat de Barcelona
B:KC Barcelona Knowledge Campus
Campus d'Excel·lència Internacional

I have no special talents. I am only passionately curious.

Albert Einstein

En primer lloc, m'agradaria agrair al Jordi per la seva implicació i dedicació, així com als integrants del laboratori 4017 per orientar-me i fer més amè aquest treball. També vull agrair la companyia dels meus amics, especialment a l'Albert, per donar-me tota la seva ajuda sempre que ho he necessitat.

A la meva mare i germana pel seu suport i viure tan de prop l'evolució d'aquest treball, però sobretot al meu pare, que, tot i que mai arribi a llegir-se'l, hauria estat el que més orgull hauria sentit i més l'hauria presumit.

REPORT

IDENTIFICATION AND REFLECTION ON THE SUSTAINABLE DEVELOPMENT GOALS (SDG)

The field of microfluidics has brought revolutionary changes in various areas, especially in sample analysis, thanks to its ability to perform complete analyses with small volumes and in a short time, thus contributing to sustainability. This reduction in time and the small quantity of samples required have improved diagnostic capacity, benefiting global health and reducing the need for invasive treatments. Besides, microfluidics has opened up opportunities to the development of new devices that enhance technological capabilities in various sectors. For instance, sensors for monitoring nutrients and contaminants in agriculture, promoting more sustainable agricultural practices.

In this work, a new methodology for determining the diffusion coefficients of substances using microfluidic devices is studied, with the aim of applying it as a practice in a laboratory. In terms of applications to promote the accomplishment of the Sustainable Development Goals, this work aspires to have a future impact on environmental sustainability (Group 3: Planet Earth's Conservation), on technological innovation (Group 2: Prosperity), as well as on human well-being (Group 1: People's Wellbeing), from two different perspectives.

On one hand, it fosters the acquisition of knowledge and the development of students' skills, providing a practical opportunity to understand and apply the principles of microfluidics and diffusion, directly contributing to quality education. This aligns with Goal 4, which describes and promotes quality education, and specifically with the objective 4.7., which aims to ensure that all learners acquire the knowledge and skills needed to promote sustainable development. This can result in the formation of skilled professionals in scientific and technological fields, making the development of this methodology a valuable tool for science and engineering education, which aligns with Goal 9, specifically, target 9.5, aiming to enhance scientific research, upgrade technological capabilities, and promote innovation.[23]

On the other hand, comprehending the physics of fluid mixing within these microsystems enables to design and optimize microdevices, allowing for the development of new microfluidic systems that contribute to the improving quality of life and environmental responsibility in various

ways. By understanding how substances diffuse in microfluidic systems, more efficient technologies for water treatment and methods to control and monitor pollution can be developed, which is associated with Goal 6, specifically with target 6.3.

This fact can be related, at the same time, to Goal 14.1, which states the prevention and reduction of marine pollution to protect underwater life.

Finally, the results of this work can also contribute to Goal 12.4, which aims to minimize adverse impacts on human health and the environment through proper management of products and waste, since it can provide knowledge that can be used to design more effective containment strategies.[23]

CONTENTS

1. SUMMARY

Microfluidics is an interdisciplinary field of science and technology based on the manipulation of fluids in systems with channels generally less than 1 mm in thickness. Microfluidic devices allow the integration of complete analytical systems in reduced spaces and, in addition, new properties unique to small-scale flows are introduced. A fundamental characteristic of these systems is the predominance of viscous forces over inertial forces. Consequently, the typical chaotic and turbulent behavior of flows in the macroscopic world is replaced by an orderly fluid motion forming parallel layers - laminar flow - which hinders mixing processes. In these microsystems, diffusion becomes the main transport mechanism, whereas it is an inefficient phenomenon at larger scales.

In this work, the predominant role of diffusion will be leveraged to develop an innovative methodology for determining diffusion coefficients using a microfluidic system, oriented to be implemented in teaching laboratories.

This system will include an injection device recently acquired by the Universitat de Barcelona that is capable of propelling fluids through microchannels under pressure. In addition, it will be computer controlled and will be observed through a microscope equipped with an ultra high-speed camera.

The diffusion coefficients of colored substances diffusing through two flows inside Y-shaped microchannels will be measured. To do so, concentration profiles along the channel will be extracted from the recorded images and diffusion times will be obtained from the flow velocity, which will be controlled by the aforementioned injection device.

Additionally, by determining the diffusion coefficients, the Einstein-Stokes equation will be verified, studying the role of solute size and solvent viscosity.

Keywords: Microfluidics, laminar flow, diffusion, diffusion coeficient.

2. RESUM

La microfluídica és un camp interdisciplinari de la ciència i de la tecnologia basat en la manipulació de fluids en sistemes amb canals amb un gruix generalment inferior a 1 mm. Els dispositius microfluídics permeten la integració de sistemes complets d'anàlisi en espais reduïts i, a més, s'hi presenten noves propietats exclusivament característiques dels fluxos a petita escala. Una característica fonamental d'aquests sistemes és el predomini de les forces viscoses per sobre de les inercials. En conseqüència, el típic comportament caòtic i turbulent dels fluxos en el món macroscòpic queda substituït per un moviment del fluid ordenat i formant capes paral·leles – flux laminar –, cosa que dificulta els processos de mescla. En aquests microsistemes, la difusió esdevé el principal mecanisme de transport, mentre que es tracta d'un fenomen ineficient a escales majors.

En aquest treball, es farà ús del paper predominant de la difusió per a desenvolupar una metodologia innovadora per determinar coeficients de difusió emprant un sistema microfluídic, orientada a poder ser implementada en laboratoris docents.

Aquest sistema comptarà amb un aparell d'injecció recentment adquirit per la Universitat de Barcelona que és capaç d'impulsar fluids per microcanals exercint pressió. A més, estarà controlat per ordinador i s'observarà a través d'un microscopi equipat amb una càmera d'alta velocitat.

Es mesuraran els coeficients de difusió de substàncies acolorides que difonen a través de dos fluxos dins de microcanals en forma de Y. Per a fer-ho, s'extrauran perfils de concentració al llarg del canal a partir de les imatges enregistrades i s'obtindran els temps de difusió a partir de la velocitat dels fluxos, que estarà controlada per l'aparell d'injecció esmentat.

A més, mitjançant la determinació dels coeficients de difusió, es verificarà l'equació d'Einstein-Stokes, estudiant el paper de la mida del solut i de la viscositat del solvent.

Paraules clau: Microfluídica, flux laminar, difusió, coeficient de difusió.

3. INTRODUCTION

Microfluidics is an interdisciplinary field of science and technology emerged in the 1980s and focused on the manipulation of fluids and the study of their behavior within integrated devices characterized by microscopic dimensions, generally below 1mm [1–4].

The distinctive features of these systems have driven the growth of this field, opening up new opportunities for both research and industry in different areas and leading to the development of new components and the implementation of new approaches for fluid manipulation within channels. For instance, the creation of integrated microfluidic devices, so-called lab-on-chips. These microfluidic devices have the potential to revolutionize how diagnostics and other laboratory processes are performed, since they integrate all the functions of a human-scale test laboratory: transferring samples, extracting a precise volume of a product, mixing with reagents, heating, etc., all within a small-sized system.[2,3,5]

Microdevices offer the benefit of requiring the use of small sample and reagent volumes, reducing analysis and reaction times, as well as enhancing sensitivity and reproducibility, leading to revolutionary changes in terms of sample analysis, chemical synthesis, and engineering. [1,2,5]

Furthermore, the fluids exhibit at the microscale different behavior compared to macroscopic systems, as a result of some phenomena becoming more relevant as size reduces, enabling the overcoming of the limitations of macrosystems and allowing methodologies that would not function on a larger scale.

The miniaturization of these systems increases the surface-to-volume ratio, making surface effects, such as capillarity or adsorption, more significant. A higher specific surface also promotes more efficient heat and mass transfer, as there is more surface area available for interaction per unit volume. Additionally, the reduction in system size causes the effects of viscosity to overcome the influence of inertia. As a consequence, the chaotic and random behavior of flow in macroscopic systems is replaced by a smooth and orderly movement of fluid layers, making mixing a challenging task. The phenomenon that emerges as the primary mechanism for blending

liquids at the microscale is diffusion, whereas at the macroscale it is an inefficient transport mechanism.[1,5,6]

Understanding the unique and distinctive characteristics of microfluidics and how they affect fluid behavior is critical for quantitatively analyzing diffusion transport and accurately determining diffusion coefficients.

3.1. LAMINAR FLOW

The most distinctive and determining feature of the behavior of microsystems is the dominance of the viscous forces, which are intrinsic intermolecular forces within the fluid that lead to internal friction, over inertial forces, forces which describe resistance of the liquid to change their state of motion. The predominance of viscosity tends to inhibit turbulence in fluid flow, causing the fluid motion to be characterized by parallel and ordered laminae and streamlines that do not get intermixed. The regime that exhibits this smooth behavior and stability to perturbations is known as laminar flow.[6–8]

The counterpart of laminar flow, which presents the typical fluid behavior known and observed in the macroscopic world, is turbulent flow. It involves an inertia-dominated regime, which displays random and unpredictable fluid motion defined by eddies, vortices, and other flow instabilities (*Figure 1*).

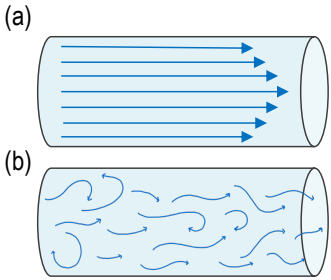

Figure 1. (a) Laminar flow and (b) turbulent flow.

The relative importance of both forces for given flow conditions, which enables the prediction of the system's behavior, can be quantified by the dimensionless Reynolds number,

$$Re = \frac{\rho v L}{\eta} \qquad \text{Eq. I}$$

Here, η represents the dynamic viscosity of the fluid, ρ corresponds to its density, v is the mean flow velocity, and L defines the characteristic length, which in microfluidic systems corresponds to the width of the channel employed.

A system characterized by a Reynolds number below 2300 can be considered laminar, whereas a regime corresponding to a Reynolds number above 4000 is turbulent. On the other hand, all systems with a number between both mentioned values are known as transitional flow regimes and exhibit an intermediate behavior.[6–8]

Owing to the small dimensions and small volumes used, in the microscopic world of microfluidics, Reynolds numbers are at the low limit, resulting in a purely laminar fluid flow, where viscous forces outweigh inertial forces.

3.2. TRANSPORT PHENOMENA IN MICROFLUIDICS

Understanding the transport mechanisms that occur in these laminar systems is essential, as most microfluidic applications require a mixing stage.

There are two main transport processes that can be responsible for blending liquids: diffusion and convection. Diffusion is a transport mechanism involving the formation of a material flux in response to a concentration gradient to achieve equilibrium, while convection is fluid motion due to a gradient in temperature, pressure or external forces, which can carry solute molecules along with it (*Figure 2*).[1,8]

Both phenomena are correlated by the dimensionless Péclet number,

$$Pe = \frac{vL}{D} \qquad \text{Eq. II}$$

Here, v represents the flow speed in the flow direction, D is the diffusion coefficient, and L corresponds to the characteristic channel size over which convection and diffusion are evaluated, usually regarded as the channel width.

Depending on the magnitude of this number, one can conclude which transport phenomenon governs each system. If the Péclet number is below 1, diffusion predominates, while if the Péclet number is above 1, the system is mostly influenced by convection.[6,7,9]

Since microfluidics deals with small-dimension systems and relatively low velocities, it can be confirmed that in the laminar regimes typical of these systems, mixing is achieved by molecular diffusion.[1,7,8]

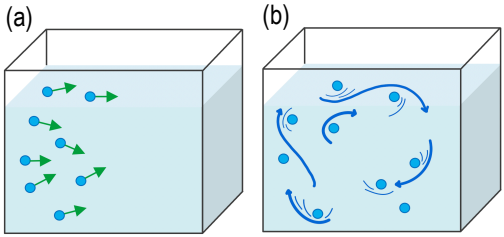

Figure 2. (a) Diffusion phenomenon and (b) convection transport (also known as advection).

3.2.1. Fundamentals of diffusion

Diffusion can be defined as the formation of a material flux in response to a concentration gradient. The origin of this flux is the random motion of individual particles due to fluctuations in thermal energy in the fluid, known as Brownian motion. It involves a statistical behavior by nature that describes the movement of a single molecule as a random walk, where the mean square displacement of a particle in a time t is characterized by the Einstein-Smoluchovski equation,[6,8]

$$\langle(\Delta x)^2\rangle = 2Dt \qquad \text{Eq. III}$$

The overall effect of this microscopic and disordered movement, by which particles move in different directions and collide, is the transport of material from a region of higher concentration to a region of lower concentration until the chemical potentials equalize (*Figure 3*). This resulting effect can be described by the First and Second Fick's laws.

The First Fick's law (*Equation IV*) is an empirical law that states that the generated flux is a function of a static (time-independent) concentration gradient, while the second Fick's law (*Equation V*), derived from the first one, predicts how diffusion changes the concentration gradient over time,

$$J = -D\frac{dC}{dx} \qquad \text{Eq. IV}$$

$$\frac{\partial C}{\partial t} = D\frac{\partial^2 C}{\partial x^2} \qquad \text{Eq. V}$$

Here, J corresponds to the material flux, t is the time diffusion, x represents the position in space, C is the concentration of the substance, and D is the diffusion coefficient.[6,8] The diffusion coefficient can be described as the ability of a substance to diffuse in a medium under given conditions, and it is characterized by the Einstein-Stokes equation,

$$D = \frac{K_B T}{6\pi\eta a} \qquad \text{Eq. VI}$$

This equation expresses the inverse correlation of the diffusion coefficient, D, of the spherical particle with a radius a that diffuses, and the dynamic viscosity, η, of the fluid at a certain temperature, T. Thus, the smaller the particle and the less viscous the medium where it is, the more rapidly the substance diffuses.

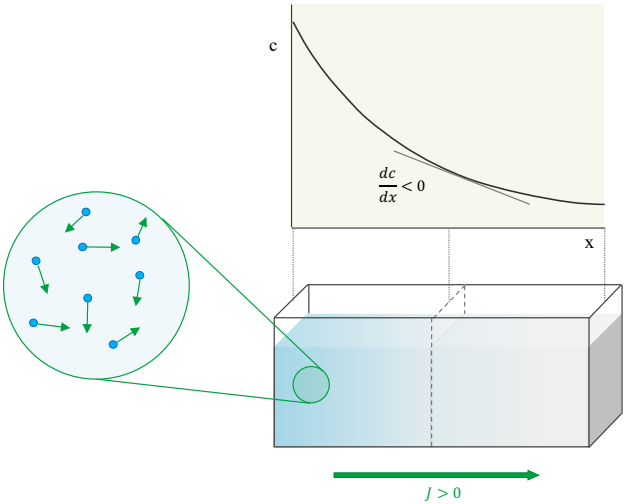

Figure 3. Diffusion at both macroscopic and microscopic levels. This illustration shows how the material flux tends to reduce the concentration gradient.

3.2.2. Diffusion in microfluidic systems: Y-junction channels

Microfluidic systems, as explained in the previous sections, are characterized by laminar flow and by the fact that molecular diffusion is the only significant mixing mechanism.

This behavior enables the examination and study of diffusion through the use of a microdevice, widely employed in the field of microfluidics, which incorporates a Y-junction channel – so named due to its Y-shaped configuration. The device features two inlet channels where two fluids are injected, converging into a main channel where both streams come into contact before exiting through a single outlet. [1]

In contrast to what is expected in the macroscopic world, where fluid mixing occurs immediately and in a chaotic manner due to turbulence, microfluidic systems operate under laminar flow, enabling fluids to travel alongside each other, forming parallel layers (*Figure 4*).[6]

In fact, the localization of the interface between the two liquids can be predicted by controlling the flow rate used to inject each of them. The fraction of channel filled by each fluid is given by the following expressions:[8]

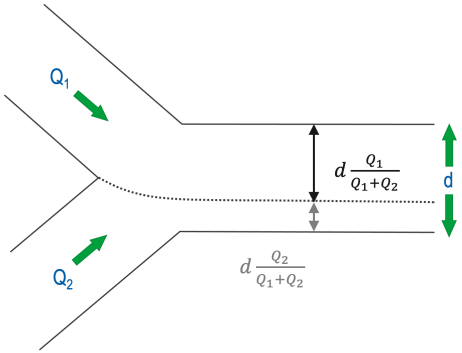

Figure 4. Domain geometries as predicted by inlet flow rates (Q1 and Q2).

Thus, if both liquids are introduced into the system at the same flow rate, the interface is situated in the center of the main channel.

When one of the introduced fluids is a solution and the other is a solvent, a concentration gradient is established, which acts as a driving force, leading to the transverse diffusion of the solute. Therefore, in accordance with Fick's laws, as the two fluids flow through the channel, diffusion occurs perpendicular to the flow direction. Figure 5 provides a clear illustration of this diffusion phenomenon and demonstrates how it increases as the fluids spend more time in contact while traveling through the channel.[5]

The second Fick's law is employed in order to mathematically describe this system. This partial differential equation can be solved for a wide variety of systems by defining appropriate boundary and initial conditions. The valid solution applicable to these microsystems is Equation VII, which defines the concentration profiles of a solute with a diffusion coefficient, D, in each position along the x-axis relative to x_o, at a given time t.

$$\frac{c}{c^o} = \frac{1}{2} erfc\left(\frac{x-x_o}{2\sqrt{Dt}}\right) \qquad \text{Eq. VII}$$

Here, $erfc(x)$ stands for the complementary error function.

In conclusion, by utilizing the provided solution, one can construct the concentration profiles at various positions along the rectilinear track.[10]

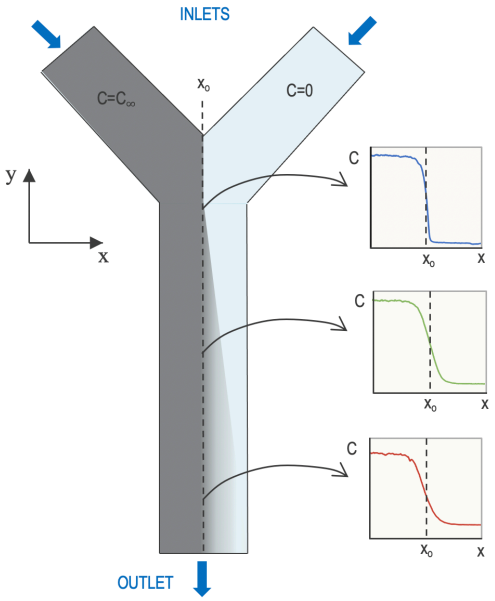

Figure 5. Introduction of a colored solution (left inlet) and a solvent (right inlet) in a Y-junction channel. Laminar flow and perpendicular diffusion can be clearly observed. At the right, the evolution of the concentration profiles at different positions along the channel.

Additionally, for a constant velocity flow, v, the diffusion time at a downstream position Δy, is

$$t = \frac{\Delta y}{v} \qquad \text{Eq. VIII}$$

allowing for the estimation of the diffusion coefficient, as will be explained later in this work.

3.3. POISEUILLE FLOW

Poiseuille flow is one of the two simplest solutions of the Navier-Stokes equation and the most common type of flow observed in long and narrow channels. This flow describes a laminar flow between fixed parallel plates driven by pressure gradients -a pressure-driven laminar flow-, resulting in a steady, incompressible, and viscous flow with a parabolic velocity profile. [8]

The Navier-Stokes equation cannot be solved analytically unless certain simplifications are made, allowing for direct integration. The simplifications enabled by the assumption of Poiseuille flow are as follows: the flow is unidirectional through a channel of infinite extent, and it is fully developed, meaning that it is far enough from the entrance and exit that no entrance effects remain. Furthermore, the convective term of the Navier-Stokes equation is negligible because the

fluid velocity and the velocity gradients are orthogonal. Hence, by imposing the flow symmetry and using the boundary conditions at each wall, Poiseuille flow can be accurately described. A more detailed mathematical description is provided in Appendix 1.[8,11]

Equation IX presents the 1D Poiseuille solution for the Navier-Stokes equation and the continuity equation. It describes a parabolic velocity profile, with the maximum velocity achieved at the center of the channel, gradually decreasing towards the walls due to friction with the plates.

$$v = -\frac{1}{2\eta}\nabla P x(h - x) \qquad \text{Eq. IX}$$

Here, η represents the dynamic viscosity, ∇P denotes the pressure gradient along the channel, h is the distance between the parallel plates and x represents the position between the plates.

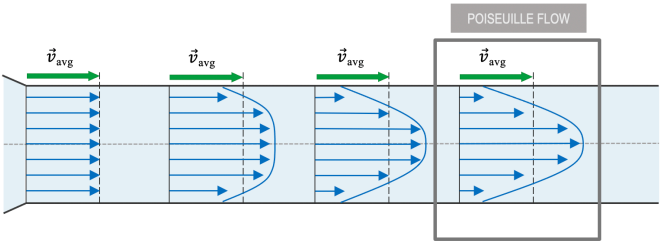

Figure 6. The establishment of the 1D Poiseuille flow in a Y-junction channel.

Poiseuille flow can be a valuable tool in the study of microfluidics systems. For instance, the parabolic velocity profile associated to Poiseuille flux is useful for predicting the distribution of fluid velocities within the channel.

4. OBJECTIVES

The main objective of this experimental work is to explore the possibility of quantifying the diffusion coefficients of colored substances as they diffuse through two laminar flows inside a Y-junction microchannel. This assignment will be undertaken preparing a new microfluidic system constituted by an injection device recently acquired by the Universitat de Barcelona (UB) and following a methodology specifically oriented to a future application in academic laboratories of physical chemistry.

In particular, the aim is to quantify the diffusion coefficients of potassium permanganate in water, as well as those of malachite green both in water and in a 50/50 (w/w) mixture of water and glycerol. This approach will enable the study of the influence of solute size and medium viscosity on the diffusion process and the evaluation of the efficacy of the method employed in this project.

5. EXPERIMENTAL SECTION

5.1. MATERIALS AND EQUIPMENT

For the microchip fabrication, the commercially available PDMS, most commonly used, Sylgard™ 184 produced by Dow Corning, has been employed. It consists of two parts – a silicon base and a curing agent.

The solutions have been prepared and filtered (Nylon membrane, 0.2 μm) using $KMnO_4$, malachite green (*Appendix 2, Figure B1*) and glycerol provided by the *Departament de Ciència de Materials i Química Física* from the Universitat de Barcelona.

In addition, various pieces of equipment have been required. A ProFluidics 285D printer (CADworks3D, Canada) has been used to print the mold and a plasma treatment device, ZEPTO (Electronic Diener, HF-Generators), has been employed to adhere the microchip to a glass surface. A Flow EZ from FLUIGENT has been used as a flow controller to propel the fluids within the microchip. The observation and data collection have been carried out using cameras (CHRONOS 2.1-HD and FLIR BFLY-PGE-50S5M-C) coupled to an optical microscope (Euromex Oxion Inverso, OX.2053-PL) and connected to a PC.

Image processing and data analysis have been performed using ImageJ, IgorPro and Microsoft Excel softwares.

5.2. METHODOLOGY

The study described in this project has been applied to an aqueous solution of potassium permanganate, an aqueous solution of malachite green, and a solution of malachite green in a 1:1 (w/w) mixture of glycerol and water.

The experiments described in this Section have been conducted at different flow injection pressures to find the ideal range that permits an accurate calculation of the diffusion coefficient. For potassium permanganate, experiments have been performed at injection pressures between 40 and 60 mbar (always referred to values above atmospheric pressure), at intervals of 5 mbar.

For both cases of malachite green, experiments have been conducted at pressures between 25 and 35 mbar, also at intervals of 5 mbar.

5.2.1. Experimental setup

In order to carry out the experiments accurately, it has been necessary to establish an experimental setup that guarantees precise and controlled fluid flow through the microchip. It incorporates various crucial components destined to sustain consistent flow rates and facilitate the process of observation and data collection.

Fluids are propelled through the chip using a flow controller device supplied by a gas source, in this case, nitrogen, and a power supply. This microfluidic pressure-based flow controller pressurizes reservoirs containing the solutions or liquids, rapidly injecting them into the microchip. This controller device ensures a stable and pulseless flow, enhancing accuracy and reproducibility in experiments. Essentially, it consists of technology that operates by controlling fluid flow through pressure monitoring.

In this project, two reservoirs have been used: one containing a solution previously filtered of the solute under study (permanganate or malachite green solution) and the other containing the solvent used to prepare the solution (water or a water-glycerol mixture). Each solution has been propelled and forced to flow into the microchip via tubes (FEP 1/16''OD 0.20''ID) through different inlets, where they finally come into contact, creating the system presented in Figure 7.

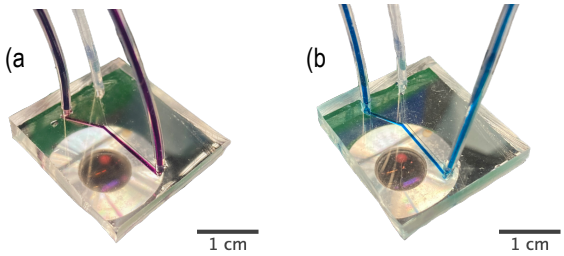

Figure 7. (a) Solution of potassium permanganate and water, and (b) solution of malachite green, coming into contact inside the Y-channel microchip, above the microscopi objective.

This system has been studied through observation using an inverted optical microscope with an attached camera, allowing for data collection.

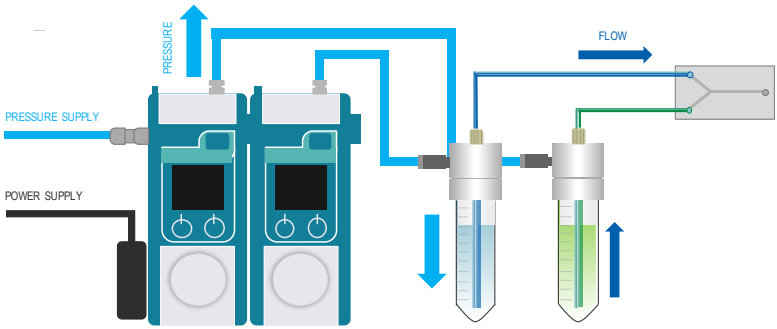

Figure 8. Experimental setup.

5.2.2. Microchip fabrication

The devices used in microfluidics are typically fabricated using the synthetic polymer Polydimethylsiloxane, PDMS. It is a member of the silicone polymer family, formed by the repetition of dimethylsiloxane units. Namely, its structure consists of a backbone of silicon atoms bonded to oxygen, where each silicon is simultaneously bonded to two methyl lateral groups, that wrap around the outside of the long chain (*Appendix 2, Figure B2*).

Due to its wide range of properties suitable for stamping and molding, which permit for cheap and easy fabrication and study of these microsystems, PDMS has become the most common material used for this application. PDMS provides a low interfacial free energy and hydrophobic surface caused by methyl groups, allowing the control over interactions with various substances. Additionally, it is chemically inert, thermally stable, non-toxic, and transparent across the optical spectrum, enabling the visualization of microchip content. Among many other properties, these factors make PDMS particularly useful for microdevices fabrication.[12–16]

For the production of these microfluidic devices, a mixture of a silicone base and a curing agent has been poured into a master mold and heated to promote and accelerate the polymerization of PDMS, resulting in an elastomeric replica of the mold.

5.2.2.1. Preparation of the master mold

As previously mentioned, PDMS is molded to achieve the desired shape using a master mold. The mold acts as a template, displaying the structure and details to be replicated by the PDMS. Therefore, the liquid polymer is poured into the master mold where polymerization takes place, adopting an elastomeric solid structure that reflects the characteristics of the mold.

Various methods have been developed and employed for the preparation of master molds, such as lithography or direct writing. The master mold used in this project has been prepared using a 3D printer and exhibits various Y-shaped channels that have been later replicated by the PDMS (*Figure 9*). It has been specifically used a UV resin 3D printer, which utilizes a technology based on the photopolymerization of a liquid resin by exposing it to UV light. This resin is composed of acrylate monomer, acrylate oligomer, photoinitiator and additives (trade secret).

The prepared mold specifically contains a total of four Y-shaped channels, each with the following dimensions: 1 mm in width, 0.5 mm in depth, and a length of 12 mm. However, even though 3D printers offer high precision, it is essential to consider factors that may cause changes in dimensions during and after the printing process, such as contractions of the resin during curing.

Once the mold is prepared, it is important to subject it to a thermal treatment in order to remove a specific solvent that contains the material used for its fabrication. If this step is not completed before adding the PDMS, this solvent covalently bonds the PDMS to the master mold, making it impossible to peel off after the curing process.

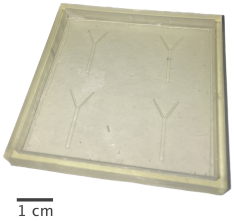

Figure 9. Master mold prepared by a 3D printer.

5.2.2.2. PDMS polymerization and curing

The preparation of PDMS consists of thoroughly mixing a liquid prepolymer and a curing agent at a ratio of 10:1 (base/ curing agent, w/w) to obtain the optimal and adequate mechanical properties. [15]

It is important to consider that the high viscosity of both components causes air entrapment during the mixing process, resulting in the formation of bubbles in the PDMS mixture. These bubbles must be removed as they can lead to structural defects and significantly decrease the strength and transparency of the resulting chips. The simple and effective method that has been

used to remove them involves reducing the pressure of the system by introducing the mixture into a vacuum desiccator.[13,14]

As previously mentioned, the preparation of the two-component mixture activates the polymerization process into de master mold, transforming the liquid polymer into a solid elastomer. This curing process has been accelerated and facilitated by heating at 80ºC during at least 4 hours. After the PDMS has cured, it has been carefully removed from the master mold, ensuring not to damage the channels or the printed features. This process is relatively straightforward, facilitated by the low free surface energy of PDMS.[14,16]

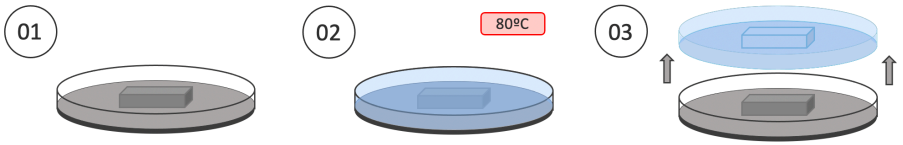

Figure 10. The process of curing PDMS in a mold and its removal from the mold.

During the curing and demolding processes, distortions of the replicated features can occur, resulting in slight variations in channel dimensions compared to the original mold. These distortions can be caused by shrinkage during the curing of PDMS, differences in thermal expansion coefficients between PDMS and the mold, or during the process of peeling the microchip off the mold. [17]

5.2.2.3. Microchip construction

The following step involves trimming any excess of polymer using a cutting tool, such as a precision cutter, or, in this specific case where multiple channels are present in the mold, separating them.

Subsequently, inlet and outlet holes have been punched to facilitate the introduction of solutions or liquids into the microchip, utilizing a biopsy punch of 1.25 mm.

At this stage, the microdevices have the channels open on one side, requiring them to be sealed. This has been achieved by adhering the devices to a glass surface, ensuring that the channels remain closed, with the only openings being the inlet and outlet holes (*Figure 11*).

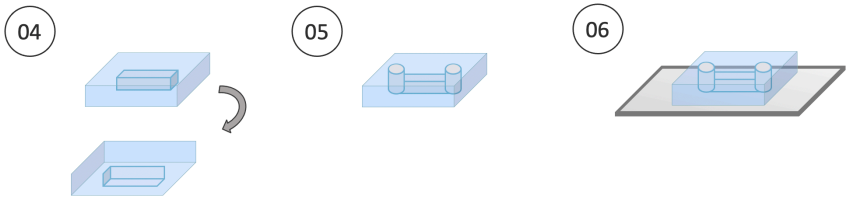

Figure 11. Final steps in the preparation of the microchip: punching holes and sealing the channels.

This process of adhesion is straightforward due to the fact that surface properties of PDMS are relatively easy to modify. Among the various methods that can be used, an oxygen plasma treatment has been chosen, as it is one of the most commonly employed methods due to its short processing time, good repeatability and consistency. [13,16]

The oxygen plasma treatment involves the use of a plasma composed of ionized oxygen at high energy to oxidize the surfaces of the PDMS chip and a glass microscope slide. This oxidation process makes the PDMS surface hydrophilic and increases the hydrophilicity of the glass surface. When the PDMS surface is oxidized, silanol terminations are produced, rendering the surface polar. [13,16,18]

As a result, when this PDMS is deposited onto the glass slide, it gets covalently bonded through the creation of Si-O-Si bonds (*Figure 12*). The formation of these bonds has been thermally promoted at 70ºC for at least 4 hours.

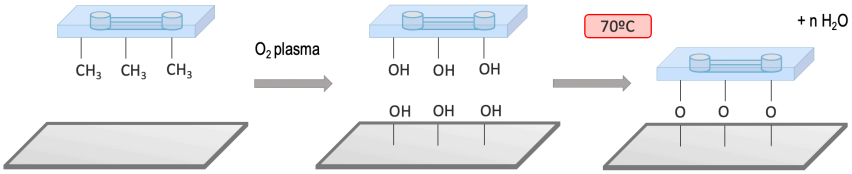

Figure 12. Increasing the hydrophilicity of the surfaces of the glass slide and PDMS to seal the channels by adhering them.

As in the previous steps, the dimensions of the channels may be slightly altered. In fact, plasma treatment tends to be the main reason.[16,19]

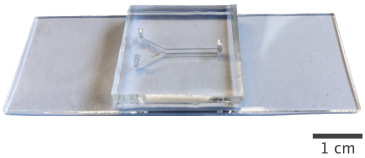

Figure 13. Microchip used in all the experiments described in this work.

5.2.3. Data collection

A method for determining the diffusion coefficient of solutes has been developed and followed, which can be divided into two stages that permit the acquisition of the necessary data for calculating the coefficient. One stage involves constructing different concentration profiles to determine the diffusion length, while the other stage consists of measuring the flow velocity to determine the diffusion time.

5.2.3.1. Concentration profiles acquisition

As mentioned previously, the microchip containing the Y-junction channel allows for the observation of diffusion evolution along the channel, facilitating the study of this transport phenomenon.

To determine the lateral diffusion coefficient of the selected substances, diffusion has been monitored by capturing images at various positions from the Y-merging point. These captured images (2448x2040 pixels) have been analyzed using ImageJ software in order to extract the concentration profiles perpendicular to the flow direction at equidistant positions along the channel. In fact, the obtained profiles represent the relative intensity of the transmitted light (gray values). Therefore, by assuming that this intensity is linearly related to concentration, the data can be fitted to the following expression obtained after resolving the differential Equation VII, when the initial condition is a step in the concentration profile:

$$I = I^o + B\ erfc(a(x - x_o)) \qquad \text{Eq. X}$$

This fitting process has been executed using IgorPro software, which provides the values of x_o, representing the center of the diffusion profile; I^o, the baseline intensity; B, referring to a constant that depends on the intensity of the microscope light; $erfc(x)$, the complementary error function; and a, which will be the most important parameter.

This latter parameter represents the inverse of the diffusion length, which is directly related to the diffusion coefficient, D (*Equation XI*). However, in order to determine D from the values of a,

the diffusion time is required. Hence, it is crucial to determine the duration of contact between the fluids that are flowing downstream along the channel, which is essentially the time allowed for the substance to diffuse at each position where a concentration profile has been recorded.

$$a^{-1} = 2\sqrt{Dt} \qquad \text{Eq. XI}$$

This diffusion time is evaluated from the flow velocity, which remains constant as the pressure applied to the system does not vary, and from the distance from the Y-junction where each concentration profile has been extracted, Δy (*Equation VIII).*

It is necessary to specify that the chosen starting point for diffusion in the channel, y_o, has not been the apex of the Y-junction, but rather the intersection point of the tangent lines to the outer walls of the inlet channels (*Figure 14*). This criterion has been used because in the region closer to the junction, laminar flow patterns may not apply due to possible disturbances resulting from the encounter between both fluids.[5]

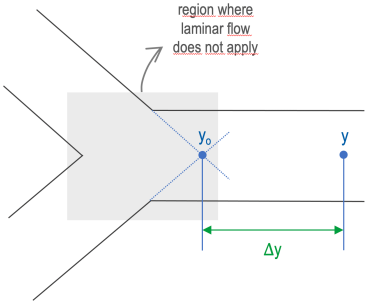

Figure 14. Approximation of the starting point for diffusion in the channel, avoiding non-laminar flow. region.

The distance from y_o can be determined either by using a position transducer attached to the microscope stage or by constructing a complete image of the channel stitching together the individual captured images and identifying the position from which the concentration profile has been extracted (*Figure 15*).

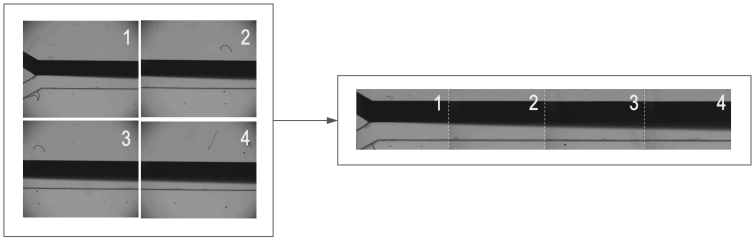

Figure 15. Construction of the complete image of the channel.

Therefore, it is necessary to measure the flow velocity to finally determine the diffusion coefficient.

5.2.3.2. Velocity measurement

A simple method for measuring the mean velocity of fluid flow within the microchannel, which does not require specific devices, such as flow meters, and is easily executable in a laboratory setting by students, involves collecting volumes at the system outlet over a determined time. This period of time must be sufficient to gather a sizable volume in order to minimize potential errors and the influence of random fluctuations, thereby improving the measurement accuracy.

In essence, volumes have been collected at the outlet while timing the collection process at different pressures, and the collected fluid has been weighted. This process enables the calculation of the system's flow rate at each pressure. Subsequently, with knowledge of the cross-sectional area of the microchip channel, the mean velocity values have been determined.

5.2.3.3. Cross-sectional area determination

Determining the linear velocity of the flow requires accurately knowing the cross-sectional area of the channel. As expounded in Section 5.2.2., various phenomena may occur during the curing, demolding and construction processes of the chip, as well as during the fabrication of the mold, which may potentially alter the dimensions of the channel. Consequently, it is crucial to determine a correction factor to adjust for this disparity in sectional area and accurately know its actual size for proper data processing. This can be achieved through various techniques, such as surface profiling using, for instance, 3D Optical Profilometer. In this project, the cross-sectional area has been determined by considering the Poiseuille solution in 1D (*Section 3.3.*).

By using this Poiseuille solution, it can be demonstrated that the maximum velocity, which is the velocity in the center of the channel, and the mean velocity of this parabolic profile are related by a factor of 3/2 (*Appendix 1*). Therefore, the linear mean velocity can be calculated from the value of the maximum velocity.

This maximum velocity has been determined at different pressures using hydrophilic polystyrene microparticles of 1.7 μm as tracers. Hence, these microparticles have been introduced into Milli-Q water, and those traveling through the center of the channel have been recorded using a high-speed camera. Subsequently, the five faster particles at each pressure

have been manually selected, and their velocity has been determined based on the frames per second (fps) used to record the video and the distance traveled within a specific number of frames.

It is important to emphasize that an ultra high-speed camera has been required due to the extremely high velocity of the microparticles. In fact, at some pressures, the particles remain imperceptible unless the video is recorded at approximately 9000 fps.

After measuring the maximum velocity, the mean values have been calculated. In sequence, in order to find the cross-sectional area from the mean flow velocity, the flow rate has been determined by collecting volumes at the system outlet over a determined time at different pressures. Given the relationship between these values and the sectional area, the latter can be calculated.

By following this procedure, a correction factor ($A_{determined}$ / $A_{initial\ design}$) has been calculated. Students can use this factor to facilitate the practice when specifically using the mold employed in this project. It is crucial to take into account that if another mold is to be used, the correction factor must be measured again.

5.2.3.4. Diffusion coefficient calculation

The diffusion coefficient has been extracted by linearly fitting the diffusion length and the square root of the diffusion time at each position along the channel. The corresponding slope of the linear representation is related to the diffusion coefficient, as shown in Equation XI.

6. RESULTS AND DISCUSSION

6.1. GENERAL CONSIDERATIONS

The criterion followed to choose the pressure used in each experiment has been based on applying a pressure low enough to ensure that the fluids move slowly within the microchip, thereby ensuring they remain in contact for a sufficient time for the diffusion mechanism to be appreciable. This not only facilitates the direct chip visualization but also enhances the data processing, as otherwise, the difference between the concentration profiles acquired along the channel is undetectable. On the other hand, it is essential for this pressure to be high enough to overcome the circuit resistance and to prevent the solute diffusion from being completed near the microchannel inlet, since this reduces the region available for concentration profiles estimation and leads to higher uncertainties, as it will be explained below.

Additionally, it has been observed that, in order to obtain consistent and reliable results, it is imperative to estimate concentration profiles in a mid-section of the channel (*Figure 16*). In other words, data should not be collected near the channel outlet, since the error function cannot accurately describe the diffusion process due to the proximity of the mixing zone to the channel wall.[5] Similarly, data extraction from the fluid inlet zone should be avoided. As it has been mentioned in Section 5.2.3., laminar behavior does not apply here, owing to the various events that occur during the initial moments of mixing zone development.[8] These disturbances cause the resulting slope of the linear fitting of a^{-1} vs. $t^{1/2}$ of the profiles extracted in this zone to be considerably smaller than the slope for the total data set obtained along the channel (*Appendix 3*). The decrease in the slope could be explained by a high Péclet number. A lower slope indicates that diffusion is not the predominant mechanism, since the slope of these representations provides the diffusion coefficient, which describes the ease with which a substance diffuses in a medium. This suggests that convection is the dominant mechanism in this region of the channel.

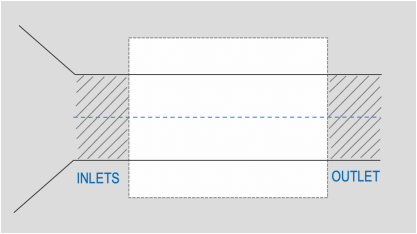

Figure 16. Area from where data should be collected.

Specifically, concentration profiles have not been obtained from the first mm of the channel, and the region of the channel beyond approximately 10 mm has been also avoided.

Another notable fact that has been observed is the necessity of filtering the solutions before performing the experiments. This is because, when dealing with very small systems and volumes, there is a high probability that the chip could become obstructed by dust particles, preventing the laminar flows from being correctly established, and resulting in systems like the ones shown in Appendix 4. Additionally, this could damage the microchip, requiring the preparation of a new one.

6.2. DIFFUSION COEFFICIENTS

6.2.1. Potassium permanganate in water

The pressure of 60 mbar has been determined as the optimal pressure for measuring the diffusion coefficient of permanganate in water.

Considering the criteria mentioned before, 12 concentration profiles describing the diffusion of permanganate in water have been extracted (*Figure 17a*). These profiles, along with the diffusion time, have facilitated the derivation of the linear fitting shown in Figure 17b.

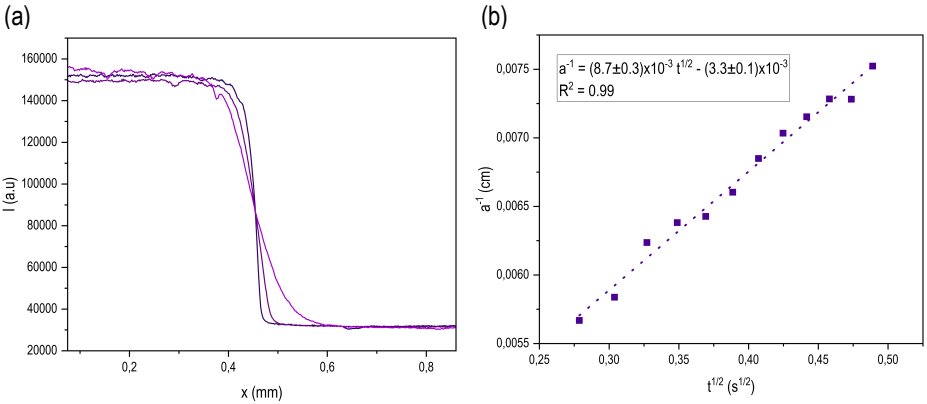

Figure 17. (a) Three of the profiles extracted for permanganate in water and (b) the linearized diffusion length vs. diffusion time, and linear fit to extract D.

Therefore, the obtained mean value of the lateral diffusion coefficient of permanganate in water is (1.8±0.1)x10^{-5} cm^2/s, at 20ºC. This value closely resembles the diffusion coefficient at infinite dilution and at 25ºC reported in the literature, D^{∞}= 1.64x10^{-5} cm^2/s [20].

It is worth noting that, as demonstrated in the Einstein-Stokes equation (*Equation VI*), at lower temperatures the diffusion coefficient decreases. This implies that, given that the experiments have been conducted at 20°C instead of 25°C, the obtained value should be lower than what is found in the literature. Moreover, the tabulated value corresponds to the coefficient at infinite dilution, which represents the upper limit of diffusion since under these conditions there are no interactions between particles that could hinder diffusion. Both facts suggest that an inflated value has been obtained.

Additionally, the determination of the diffusion coefficient enables the estimation of the hydrodynamic radius using the Einstein-Stokes equation (*Equation VI*), resulting in a value of approximately $(1.14 \pm 0.06) \times 10^{-1}$ nm, which is lower compared to the one calculated from the diffusion coefficient reported in the literature, 1.50×10^{-1} nm.

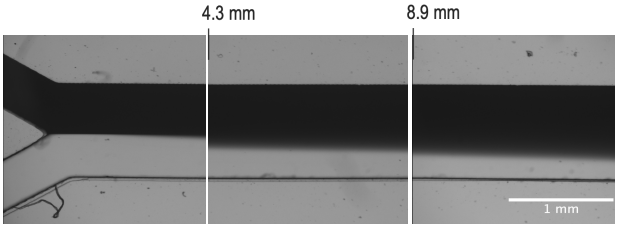

Figure 18. Y-junction channel where the $KMnO_4$ solution and water converge, resulting in the observable diffusion of MnO_4^-.

6.2.1. Malachite green

6.2.1.1. Diffusion in water

The diffusion coefficient of malachite green has been determined using a pressure of 30 mbar (see below for a discussion on this lower pressure value).

The acquisition of the corresponding concentration profiles (*Figure 19a*) has allowed for the determination of its coefficient by using the slope of the linear fit shown in Figure 19b. As a result, a value of $D = (6.8 \pm 0.5) \times 10^{-6}$ cm^2/s has been obtained for the diffusion coefficient of malachite green in water at 20ºC.

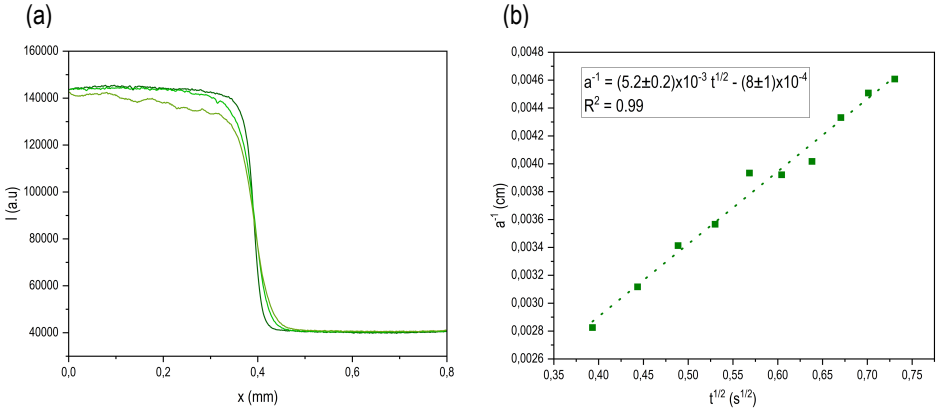

Figure 19. (a) Three of the profiles extracted for MG in water and (b) the linearized diffusion length vs. diffusion time, and linear fit to extract D.

This value is considerably lower compared to the one obtained for the permanganate anion, attributed to its greater hydrodynamic radius, by virtue of Einstein-Stokes equation (*Equation VI*). Using this equation, a radius of $(3.2\pm0.2)x10^{-1}$ nm has been obtained.

Because of the lower D, a lower pressure has been required, since a lower diffusion coefficient means that the fluids need to remain in contact for a longer time to make the diffusion process perceptible. However, as can be observed in Figure 20, even though the fluids flow through the microchip more slowly, the diffusion is much less noticeable than in the case of permanganate. Therefore, this pressure should ideally be decreased even further, but this has not been possible, as a minimum pressure of 20–25 mbar is required to overcome the resistance of the circuit and propel the fluids through the system.

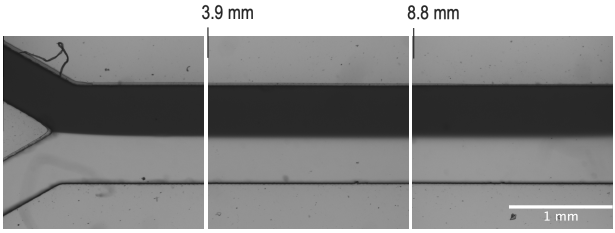

Figure 20. Y-junction channel where the MG solution and water converge, resulting in the observable diffusion of MG.

6.2.1.2. Diffusion in a mixture of water and glycerol, 50/50 (w/w)

The adequate pressure for estimating the diffusion coefficient of malachite green in a mixture of water and glycerol 50/50 (w/w) is 30 mbar (see below for a discussion on this pressure value).

Some of the 12 concentration profiles that have been extracted and the linear fitting representation are presented in Figure 21a and Figure 21b, respectively.

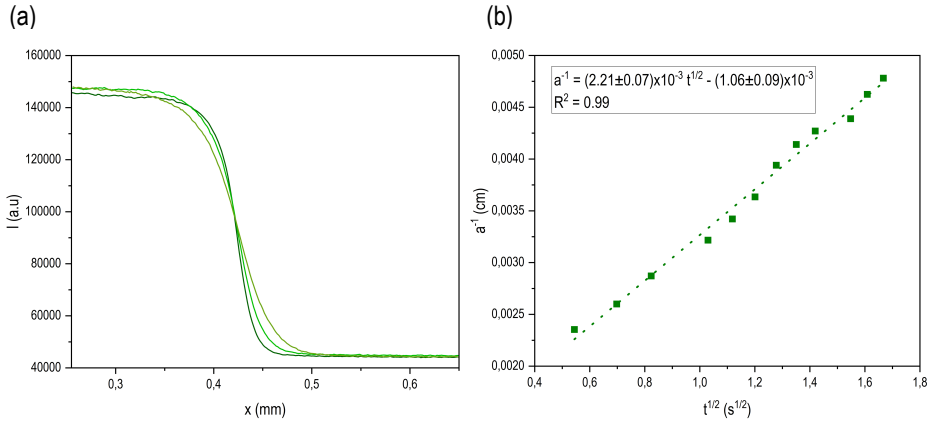

Figure 21. (a) Three of the profiles extracted for permanganate in water/glycerol mixture and (b) the linearized diffusion length vs. diffusion time, and linear fit to extract D.

Upon analyzing this data, a value of (1.22±0.08)x10^{-6} cm^2/s has been obtained for the diffusion coefficient at 20ºC. It is evident that this value is lower than that observed for malachite green in water. This observation aligns with the predictions of the Einstein-Stokes equation, which illustrates that higher viscosity in the medium corresponds to a lower diffusion coefficient.

Given that the dynamic viscosity of a 50/50 mixture of glycerol and water is 6 cP [21] compared to 1 cP for water alone, one would expect the diffusion coefficient to be six times smaller for the more viscous system. Experimentally, a factor of 5.6±0.5 has been calculated between the diffusion coefficients obtained for malachite green in water and in water/glycerol (*Equation XII*). This result further reinforces the efficacy of the methodology employed.

$$\frac{D_{MG\ in\ water}}{D_{MG\ in\ water/glycerol}} = 5.6 \pm 0.5 \qquad \text{Eq. XII}$$

Similarly to the previous two cases, the hydrodynamic radius can be estimated using the Einstein-Stokes equation, which yielded a value of (3.0±0.2)x10^{-1} nm. This value coincides with the radius obtained for malachite green in the water system within the limits of error, indicating that there are no significant changes in the size of its solvation sphere due to the decrease in solvent polarity when glycerol is added.[22]

On the other hand, even though one might expect that a lower pressure is needed given that the diffusion coefficient is smaller, as in the previous case, this is countered by the fact that the

viscosity of this system is higher. In general, for more viscous fluids, a higher pressure is required to achieve the same flow rate as for less viscous fluids. This is because the velocity of a fluid traveling through a channel is intimately linked to its viscosity. In essence, viscosity acts as a resistance to flow, impeding the fluid's movement. Hence, a fluid with a higher viscosity encounters greater resistance, resulting in a decrease in its velocity, which causes prolonged contact between the fluids. This phenomenon can be explained by the Poiseuille equation (*Equation IX*) described in Section 3.3.

Therefore, although the diffusion coefficient for this system is lower, lower pressures are not required compared to the system with only water. However, as observed in the previous case, it would be better to slightly decrease the pressure to make diffusion more noticeable. Unfortunately, this is not possible as the pressure is almost already at the minimum required to overcome the circuit's resistance.

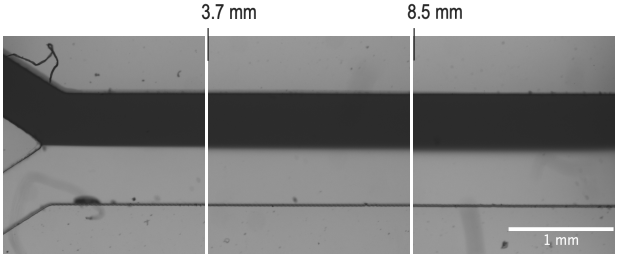

Figure 22. Y-junction channel where the MG solution and a water/glicerol mixture converge, resulting in the observable diffusion of MG.

6.3. FLOW VELOCITY

6.3.1. Flow rate measurements

As detailed in the experimental section, volumes have been collected at the system outlet over a specific time period, facilitating the subsequent calculation of velocity values necessary for determining diffusion coefficients.

The described procedure has been conducted for both the system employing water as the solvent and the system employing a mixture of water and glycerol as the solvent. This is required for both systems because, as previously explained, at the same pressure, the fluid moves at different velocities depending on its viscosity.

Figures 23a and 23c depict the representation of the flow rates and velocities obtained for the aqueous system at the study pressures of both permanganate in water and malachite green in water. In contrast, Figures 23b and 23d show the representations obtained for the more viscous system, performed at the pressure at which the coefficient of malachite green in the glycerol-water mixture has been studied.

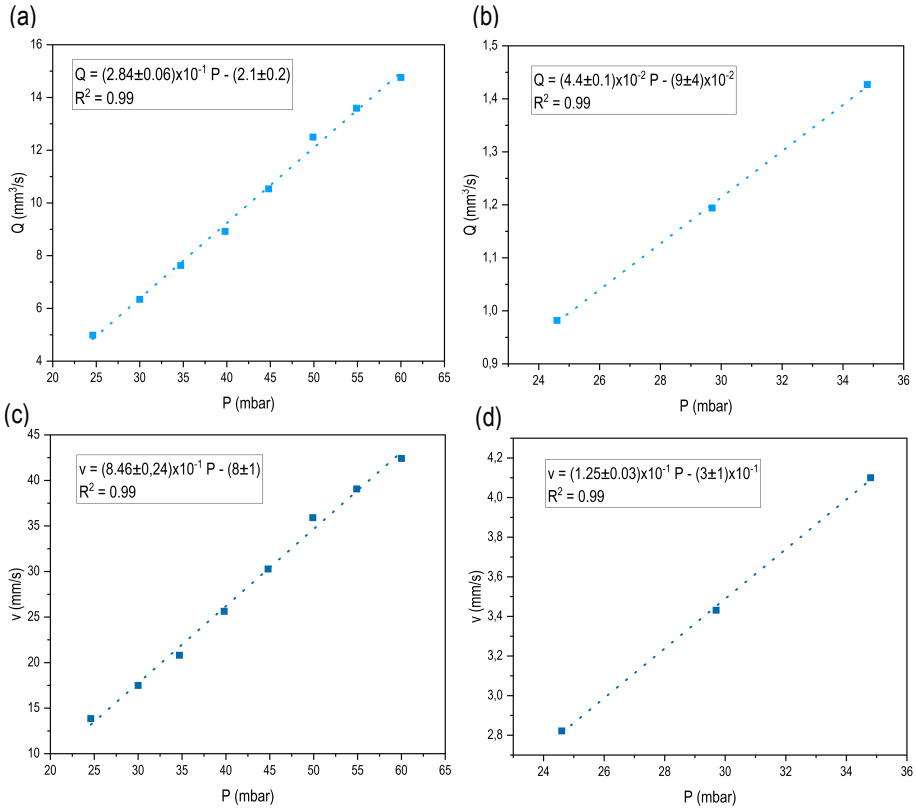

Figure 23. Flow rate as a function of the pressure applied to the (a) microsystem using only water and (b) microsystem using the mixture of glycerol and water, 50/50 (w/w). Velocity as a function of the pressure applied to the (c) microsystem using only water and (d) microsystem using the mixture of glycerol and water, 50/50 (w/w).

These graphical representations allow us to confirm the lower velocities exhibited by the more viscous system, as could be predicted.

Furthermore, all four graphs exhibit a linear relationship, consistent with the Poiseuille solution equation, which illustrates a direct proportionality between velocity and pressure drop (*Equation*

XIII). The proportionality constant relating flow rate, Q, and pressure, ΔP, is known as hydrodynamic resistance, R_h.[8]

$$\Delta P = R_h\, Q \qquad \text{Eq. XIII}$$

This resistance is an intrinsic property of the geometry channel and properties of the fluid, describing how they affect its ability to flow through the channel. It is analogous to the electrokinetic resistance described by Ohm's law, but it differs in that it is not governed by current intensity but by factors such as fluid viscosity, channel shape, and the forces involved in its movement. Hence, from the slopes of 23a and 23b, it has been possible to define a hydrodynamic resistance of 3.52 ± 0.07 mbar s mm^{-3} for the aqueous systems and a hydrodynamic resistance of 22.7 ± 0.5 mbar s mm^{-3} for the system using glycerol. These data are consistent with the theory previously discussed regarding the higher resistance to flow offered by more viscous fluids.

Upon carefully analyzing these representations, it can be observed that their fitting lines do not pass through the point (0,0). This fact can be attributed to the existence of the mentioned threshold pressure needed to overcome the resistance of the circuit and drive fluids through the system, causing the pressure to take on a certain value at the Q=0 limit. However, extrapolating these lines does not provide reliable values for the threshold pressures, presumably due to a loss of linear behavior at lower pressures.

Another significant consideration is the importance of collecting sufficiently large volumes (5-10 mL). Otherwise, errors become significantly greater, rendering this linear relationship unobservable. This entails very large periods of time, even exceeding 1 hour in some cases, particularly in the case of a solvent with a higher viscosity. In practical terms, this time-consuming calibration could also be made available to students in the laboratory, since it should be valid for a given type of devices and for a given fluid viscosity.

6.3.2. Cross-sectional area

As explained in the Experimental Section, the maximum velocity of the fluid has been measured using microparticles as tracers. The velocities of these microparticles as a function of the pressure applied to the system are represented in Figure 24.

This representation depicts a linear relationship, which can also be described using the equation for Poiseuille flow (*Equation IX*).

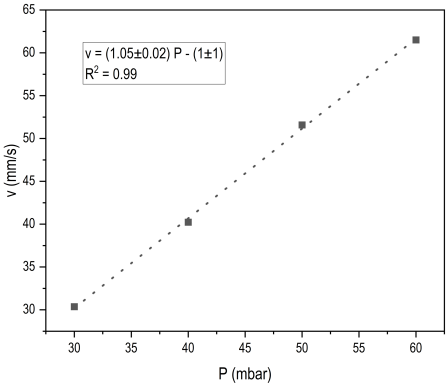

Figure 24. Velocity measured of the microparticles as a function of the pressure applied to the system.

It is crucial to ensure that the microparticles under study are those traveling in the center of the channel, not only in terms of width, but also in depth. This involves focusing the microscope on the plane corresponding to the midpoint of the channel height and maintaining it during the measurements at all pressures. Otherwise, particles traveling slower could be accidentally selected, potentially leading to a non-linear relationship.

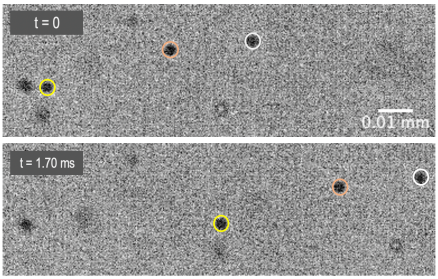

Figure 25. Distance travelled by microparticles over a determined time, propelled at a pressure of 30 mbar. Three of the particles are highlighted with a yellow, an orange and a white circle.

Finally, following the procedure specified previously in this work, a cross-sectional area of 0.35 ± 0.03 mm^2 has been determined, compared to the nominal design of 0.500 mm^2. Thus, the correction factor is 0.70 ± 0.06. This reaffirms that the mentioned phenomena occurring during the preparation of the microchip, from the fabrication of the mold to the final assembly, have a significant effect on the final dimensions of the channel that must be taken into consideration. For this reason, it is relevant to perform this kind of calibration every time a new mold is used in order to determine diffusion coefficients by following this protocol.

7. CONCLUSIONS

In this work, the effectiveness of a method for determining the diffusion coefficients of colored substances using Y-junction microfluidic devices has been demonstrated. This has been achieved by determining the diffusion coefficient of permanganate in water, malachite green in water, and malachite green in a mixture of glycerol and water, 50/50 (w/w).

On the one hand, obtaining the diffusion coefficient of permanganate has allowed for comparison with a value reported in the literature, leading to the conclusion that the values obtained with this method are consistent in terms of order of magnitude but do not provide exact values. Specifically, it seems to provide slightly overestimated values. This could be due to the method's sensitivity to various factors that may alter the specific value obtained, such as possible obstructions or changes in the cross-sectional area during microchip fabrication.

On the other hand, obtaining the diffusion coefficients of the malachite green has enabled the observation of changes in these coefficients based on viscosity and particle size parameters, revealing a clear decrease in the diffusion coefficient with an increase in both parameters, as described in the Einstein-Stokes equation.

Both facts, the obtention of coefficients of the correct order of magnitude and the accurate reproduction of the changes related to the mentioned parameters, assert that this method represents a good option to implement in physical chemistry teaching laboratories, where the aim is to promote a better understanding of the fundamentals of diffusion. Furthermore, it permits the study of diffusion not only from a mathematical point of view but also through the direct observation of the microchip, facilitating a more effective attainment of knowledge.

This method also offers the opportunity to introduce the world of microfluidics, which has been absent until now in teaching laboratories, allowing for the observation of its characteristic features, such as laminar flow.

8. REFERENCES AND NOTES

1. TAN J. N., NEILD A., *Microfluidic mixing in a Y-junction open channel*, AIP Adv, 2(032160), **2012**, p. 1-11.
2. WEIGL BERNHARD H., YAGER P., *Microfluidic diffusion-based separation and detection*, Science, 283(5400), **1999**, p. 346-347.
3. WHITESIDES G. M., *The origins and the future of microfluidics*, Nature, 442, **2006**, p.368-373.
4. TABELING P., *Introduction to Microfluidics*, Oxford University Press, **2023**, p. 1-349.
5. BINDA L., BOLADO M., D'ONOFRIO A., *Analysis of a microfluidic device for diffusion coefficient determination of high molecular weight solutes detectable in the visible spectrum*, European Physical Journal, 45(56), **2022**, p.1-11.
6. GESCHKE O., HENNING K., TELLEMAN, P., *Microsystem Engineering of Lab-on-a-Chip Devices*, Wiley-VCH, **2004**, p-13-37.
7. SEIFFERT S., THIELE J., *Microfluidics: Theory and Practice for Beginners*, Walter de Gruyter, **2020**, p.1-72.
8. KIRBY B. J., *Micro- and Nanoscale Fluid Mechanics*, Walter de Gruyter, **2010**, p.1-92.
9. RAPP B. E., *Microfluidics: Modeling, Mechanics and Mathematics*, Elsevier, **2023**, p. 3-7.
10. BURRIEL P., IGNÉS-MULLOL J., CLARET J., SAGUÉS F., *Two-Dimensional Microfluidics Using Circuits of Wettability Contrast*, Langmuir, 26(7), **2010**, p.4613-4615.
11. VÁZQUEZ R., TRÉLAT E., CORON J. M., *Stable Poiseuille Flow Transfer for a Navier Stokes System*, IEEE, **2006**, p. 775-780.
12. AKTHER F., YACOB S. B., NGUYEN N., TA H. T., *Surface Modification Techniques for Endothelial Cell Seeding in PDMS Microfluidic Devices*, Biosensors, 10(11), **2020**, p.182.
13. DUCHEYNE P., HEALY K. E., GRAINGER D. W., et al. *Comprehensive Biomaterials*, Elsevier, **2011**, p. 349-577.
14. RAMASAMY M., BRANDON H., PHAN C., et al., *Inexpensive and rapid fabrication of PDMS microfluidic devices for biological testing applications using low cost commercially available 3D printers*, Journal of Micromechanics and Microengineering, 33(10), **2023**, p.105016.
15. TSAO C. W., *Polymer microfluidics: Simple, low-cost fabrication process bridging academic lab research to commercialized production*, Micromachines, 7(12), **2016**, p. 225.
16. MIRANDA I., SOUZA A., SOUSA P., et al., *Properties and applications of PDMS for biomedical engineering: A review*, Journal of Functional Biomaterials, 13(1), **2021**, p. 2-20.
17. MADSEN M. H., FEIDENHANS'L N. A., HANSEN P. E., et al., *Accounting for PDMS shrinkage when replicating structures*, Journal of Micromechanics and Microengineering, 13(1), **2014**, p. 127002.

18. MAJI D., LAHIRI S. K., DAS S., *Study of hydrophilicity and stability of chemically modified PDMS surface using piranha and KOH solution*, Surface and Interface Analysis, 44(1), **2012**, p.62-69.
19. WEI, X., SYED A., MAO P., HAN J., SONG Y. A., *Creating sub-50 Nm nanofluidic junctions in PDMS microfluidic chip via self-assembly process of colloidal particles,* Journal of Visualized Experiments, 109, **2016**, p. 1-9.
20. HAYNES W. M., LIDE D. R., BRUNO T. J., *CRC Handbook of Chemistry and Physics 95th Ed.,* CRC Press, **2014-2015**, p. 5.77-5.79.
21. SEGUR J. B., ODERSTAR H. E., *Viscosity of Glycerol and Its Aqueous Solutions*, Ind Eng Chem, 43 (9), **1951**, p. 2119.
22. WOHLFARTH C., *Dielectric constant of the mixture (1) water; (2) propane-1,2,3-triol*, Landolt-Börnstein - Group IV Physical Chemistry 17 (Supplement to IV/6), Springer-Verlag, **2008**.
23. United Nations, Department of Economic and Social Affairs: Sustainable development, https://sdgs.un.org, **2022**.

9. ACRONYMS

1D: Unidimensional.

PDMS: Polydimethylsiloxane.

FEP: Fluorinated Ethylene Propylene.

OD: Outer diameter.

ID: Inner diameter.

3D: Tridimensional.

UV: Ultraviolet.

MG: Malachite green.

APPENDICES

APPENDIX 1: POISEUILLE FLOW SOLUTION

As it has been introduced in Section 3.3., the Navier-Stokes equation cannot be solved analytically unless certain simplifications are made, allowing for direct integration. One of its simplest solutions describes a parabolic velocity profile of a laminar flow between fixed parallel plates driven by pressure gradients, known as Poiseuille flow.

This appendix will describe how to arrive at this solution using Navier-Stokes equation and the continuity equation and what simplifications and considerations need to be made to achieve it.[8]

For its solution, a steady, laminar, incompressible, and viscous flow is considered between fixed parallel plates separated by a distance h.

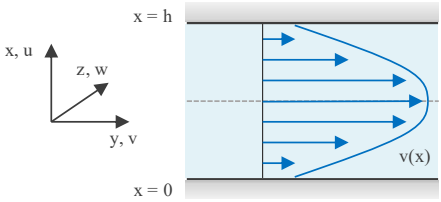

Figure A1. Laminar flow between two fixed parallel plates and its parabolic velocity profile.

These plates are assumed to be wide and long, resulting in a purely 1D flow where there are no significant components in directions other than parallel to the channel axis. Therefore, the continuity equation for incompressible fluids, which states the conservation of mass in a flux system,

$$\frac{\partial v}{\partial x} + \frac{\partial u}{\partial y} + \frac{\partial w}{\partial z} = 0 \qquad \text{Eq. A1}$$

can be simplified by removing the velocity components x and z, showing that v is not changing in the y-direction:

$$\frac{\partial v}{\partial y} = 0 \qquad \text{Eq. A2}$$

It is relevant to outline that this state is only valid for fully developed flows, which means that fluids are far enough from the inlets or outlets that no entrance or exits effects exist, which could change their velocity in the y-axis (*Figure 6*).

This allows for one of the simplifications of the Navier-Stokes equation for a 1D flow traveling in the y-direction,

$$\rho\left(\frac{\partial v}{\partial t}+u\frac{\partial v}{\partial x}+v\frac{\partial v}{\partial y}+w\frac{\partial v}{\partial z}\right)=-\frac{\partial P}{\partial y}+\eta\left(\frac{\partial^2 v}{\partial x^2}+\frac{\partial^2 v}{\partial y^2}+\frac{\partial^2 v}{\partial z^2}\right)+\rho g y \quad \text{Eq. A3}$$

where the partial derivatives of the velocity with respect to the y-axis are set to 0. Additionally, other terms can also be removed, leading to Equation A4.

- $\frac{\partial v}{\partial t}=0$, as we are considering a steady flow, meaning it does not vary over time.
- $\frac{\partial v}{\partial y}=0$ and $\frac{\partial^2 v}{\partial y^2}=0$, as mentioned before, the flow is fully developed, meaning that v does not change in the y-direction.
- $u\frac{\partial v}{\partial x}=0$ and $w\frac{\partial v}{\partial z}=0$, since we are considering a 1D flow, so there is no x or z component of velocity.
- $\frac{\partial^2 v}{\partial z^2}=0$, as we are considering no flow in z direction.
- $\rho g y$, gravity is neglected, since gravity forces are not predominant in microfluidics.

$$\frac{\partial P}{\partial y}=\eta\frac{\partial^2 v}{\partial x^2} \quad \text{Eq. A4}$$

Thus, by integrating the ordinary differential equation (ODE) obtained with respect to x, v can be written as,

$$v=\frac{1}{\eta}\left(\frac{dP}{dy}\right)\frac{x^2}{2}+C_1\,x+C_2 \quad \text{Eq. A5}$$

where C_1 and C_2 are integration constants to be determined by the application of the boundary conditions at the two plates.

Then, by applying the no-slip conditions at the lower and upper walls where velocity is by definition zero,

$$(v)_{x=0}=0 \quad \text{and} \quad (v)_{x=h}=0 \quad \text{Eq. A6}$$

yields

$$C_1=-\frac{h}{2\eta}\left(\frac{dP}{dx}\right) \quad \text{and} \quad C_2=0 \quad \text{Eq. A7}$$

and so, the solution to Poiseuille flow is

$$v = -\frac{1}{2\eta}\left(\frac{dP}{dy}\right)x(h-x) \qquad \text{Eq. A8}$$

Given that the velocity distribution in the fluid is parabolic with a maximum velocity on the centerline, v_{max} can be defined as

$$v_{max} = (v)_{x=h/2} = \frac{h^2}{8\eta}\left(-\frac{dP}{dy}\right) \qquad \text{Eq. A9}$$

On the other hand, the flow rate, Q, is

$$Q = \int_0^h v\,dx = \frac{h^3}{12\eta}\left(-\frac{dP}{dy}\right) \qquad \text{Eq. A10}$$

so that the average velocity of the flow, $\bar{v}$, is

$$\bar{v} = \frac{h^2}{12\eta}\left(-\frac{dP}{dy}\right) \qquad \text{Eq. A11}$$

From Equations A9 and A11, it can be stated that the average velocity is 3/2 of the maximum velocity reached in the center of the channel.

$$v_{max}/_{\bar{v}} = 3/2 \qquad \text{Eq. A12}$$

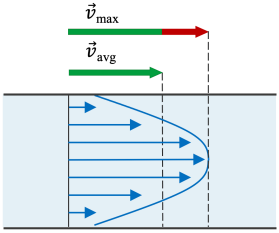

Figure A2. Average and maximum velocity of the parabolic profile of Poiseuille flow.

APPENDIX 2: STRUCTURES OF CHEMICAL COMPOUNDS

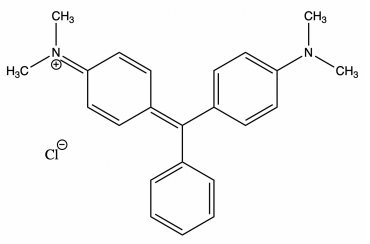

Figure B1. Malachite green structure.

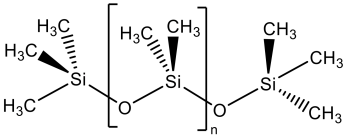

Figure B2. PDMS structure.

APPENDIX 3: BEHAVIOR IN THE VICINITY OF CHANNEL INLETS

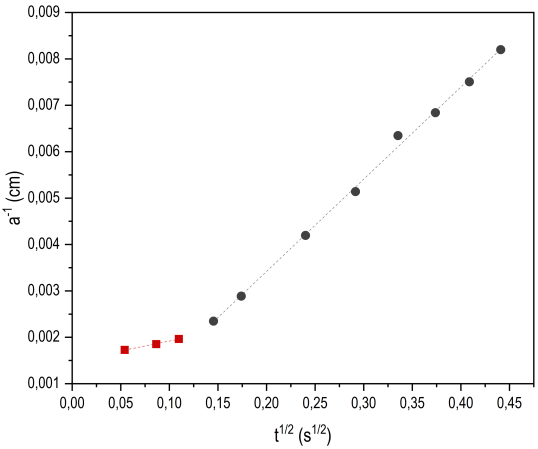

Figure C1. Data extracted from a system using potassium permanganate in water propelled by applying 50 mbar. In red, the data extracted from the first millimeter of the channel is displayed, while in gray, the data extracted from the middle section of the channel is shown. This figure clearly shows a lower slope for the first region.

APPENDIX 4: EFFECTS OF DUST OBSTRUCTIONS IN Y-JUNCTION MICRODEVICES

The presence of dust in the microchannels can cause obstructions, as shown in Figure D1, where the inlet for the potassium permanganate solution is blocked, preventing it from reaching the main channel and coming into contact with the water entering through the other inlet.

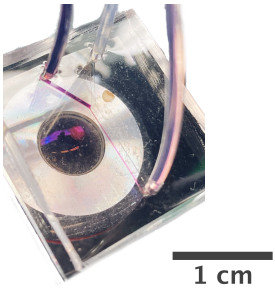

Figure D1. Total obstruction of the left inlet due to the presence of dust.

However, dust does not always cause a complete blockage; sometimes it merely interferes with the proper establishment of laminar flows, as shown in Figure D2. As it has been explained in Section 3.2.2., if both liquids are introduced into the system at the same flow rate, the interface should be situated in the center of the main channel, which is not the case here.

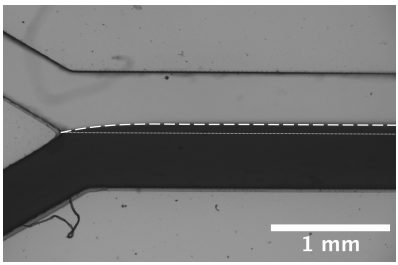

Figure D2. Improper establishment of laminar flows.

APPENDIX 5: CALCULATION OF THE ERRORS

Errors in the diffusion coefficients, the hydrodynamic radius, the hydraulic resistance, and the ratio between $D_{MG\ in\ water}$ and $D_{MG\ in\ water/glycerol}$ have been estimated using the combined uncertainty formula, which states that for a function $f(x_1, \dots, x_n) = y$, where y is a variable dependent on n known variables, with associated uncertainties δx_1,..., δx_n, the uncertainty of y is

$$\delta y = \sqrt{\sum_{i=1}^{n} \left(\frac{\partial f}{\partial x_i}\right)^2 \delta {x_i}^2} \qquad \text{Eq. E1}$$

Next, the derivation of the formula for calculating the error of the hydrodynamic radius using the combined uncertainty approach will be outlined as an exemplification.

Given that

$$a = \frac{k_B T}{6 D \eta \pi} \qquad \text{Eq. E2}$$

from the Einstein-Stokes equation; and considering the uncertainties (errors) of the diffusion coefficient, temperature (with a thermometer precision of 0.1ºC), and viscosity (extracted from the corresponding article, 1%) to be non-negligible,

$$\delta a = \sqrt{\left(\frac{\partial a}{\partial D}\right)^2 \delta D^2 + \left(\frac{\partial a}{\partial T}\right)^2 \delta T^2 + \left(\frac{\partial a}{\partial \eta}\right)^2 \delta \eta^2} \qquad \text{Eq. E3}$$

the error of the hydrodynamic radius, δa, can be calculated using the following expression:

$$\delta a = \sqrt{\left(\frac{-k_B T}{6\pi\eta D^2}\right)^2 \delta D^2 + \left(\frac{k_B}{6\pi\eta D}\right)^2 \delta T^2 + \left(\frac{-k_B T}{6\pi D \eta^2}\right)^2 \delta \eta^2} \qquad \text{Eq. E4}$$

The same procedure has been followed in order to calculate the errors of the other parameters mentioned.